RESEARCH ARTICLE | DECEMBER 12 2022

Effect of mole weight ratio of reaction on propagation of cellular detonations

Haoyang Li (李昊洋); Kepeng Yao (姚克鹏); Ruixin Yang (杨瑞鑫); ... et. al

AIP Advances 12, 125011 (2022)
https://doi.org/10.1063/5.0092993

Effect of mole weight ratio of reaction on propagation of cellular detonations

Cite as: AIP Advances 12, 125011 (2022); doi: 10.1063/5.0092993
Submitted: 25 March 2022 • Accepted: 19 November 2022 •
Published Online: 12 December 2022

Haoyang Li (李昊洋),[1,2] Kepeng Yao (姚克鹏),[1,2] Ruixin Yang (杨瑞鑫),[1,2] and Chun Wang (王春)[1,a)]

AFFILIATIONS

[1] State Key Laboratory of High Temperature Gas Dynamics, Institute of Mechanics, Chinese Academy of Sciences, Beijing 100190, China
[2] School of Engineering Sciences, University of Chinese Academy of Sciences, Beijing 100049, China

[a)] **Author to whom correspondence should be addressed:** wangchun@imech.ac.cn

ABSTRACT

The propagation of two-dimensional cellular detonations is investigated numerically using a one-step reversible reaction model. The effect of the average mole weight ratio W_B/W_A of the product and reactant on the one-dimensional Zeldovich–von Neumann–Döring (ZND) detonation and cellular detonation behavior is analyzed in detail. Several interesting cellular detonation phenomena are observed in the numerical simulations. These can be divided into five categories according to the cell patterns of detonation, i.e., regular, relatively regular, irregular, half-cell propagating, and decoupled detonation. The results indicate that differences in cell size under different values of W_B/W_A modify the cellular detonation behavior. The ZND detonation parameters under various W_B/W_A values are studied and related to the cell size. The results show that the reaction zone length and maximum heat release rate are clearly influenced by W_B/W_A. Furthermore, for both ZND detonation and cellular detonation, the reaction zone length decreases as W_B/W_A increases, which effectively reduces the cell size. To elucidate the effects of the reaction zone length on cell size, thermoacoustic instability theory is introduced to investigate the acoustic perturbations in the reaction zone. This allows the correlation between the propagation frequency and cell number along the width of the duct to be determined. Correlation analysis indicates that the cell number has a strong linear dependence on the perturbation frequency.

I. INTRODUCTION

Detonation wave is a kind of combustion wave propagating with hypersonic speed.[1–4] In reality, detonation waves exhibit complex temporal and spatial behaviors during their initiation and propagation in well-premixed detonable media. Various experiments have shown that transverse waves propagate along the detonation front and form complex multi-wave structures.[5–8] After the combustion of the detonation wave, cellular structures can be identified by the smoke foil on the wall.[9] The cell size of these cellular detonation wave artifacts inevitably depends on the properties of the premixed detonable fuel mixture.[10,11] Thus, the size of these cells can be used to correlate the critical initiation energy and the critical diameter of the detonation wave. Lee[12] conducted numerous experiments on the cell size produced by the detonation of hydrogen fuel and hydrocarbon fuel in oxygen and air. Several correlations between the detonation cell size and the critical initiation energy/critical diameter were established. For example, the work of Knystautas *et al.*[13] showed that the critical diameter of detonation is ~13 times the detonation cell size (cell width), based on results covering various combustible mixtures with hydrogen or hydrocarbon fuel under different fuel equivalent ratio conditions. By studying the energy loss and momentum loss in the reaction-inducing area, Frolov and Gel'fand[14] established the empirical criterion for the limiting diameter of gas detonation.

The chemical reaction mechanism has a great effect on the precision of simulating the detonation process. Computations with elementary mechanisms are the most accurate method, but they are computationally expensive.[15] Relatively simplified mechanisms such as two-step models obtain a good balance between computational cost and precision, so they are widely used in simulations of cellular detonation,[16,17] oblique detonation,[18–21] and so on.[22–26] The dependence of the cell size of gaseous detonation on the chemical reaction kinetics has attracted considerable attention from researchers in the field of detonation. Both simplified chemical reactions[27–31] and

elementary chemical reactions[32–38] have been introduced to numerical studies on the effect of the chemical reaction model on the detonation cell size.

Oran *et al.*[27] adopted a one-step model to simulate the propagation of the detonation and obtain a clear cell structure, while Westbrook *et al.*[28–30] simulated detonations using a one-step model to determine the optimal model parameters. Taileb *et al.*[31] studied the influence of the equation of state on the cellular structure of gaseous detonations using a one-step model and found that real gas effects alter the multi-cellular structure of gaseous detonations at elevated pressures. Oran *et al.*[32] studied the evolution process of the cell structure using a detailed reaction mechanism and found that the activation energy and pre-exponential factor are key components in determining the detonation cell structure. Shchelkin and Troshin[33] first proposed that the cell width measured in experiments may be related to the reaction length. Gavrikov *et al.*[34] analyzed the relationship between the characteristic reaction length and the width of the detonation cell through numerical simulations using a detailed reaction mechanism. They concluded that the width of the cell and the characteristic reaction length can be related by a formula under specific conditions. Eaton *et al.*[35] adopted this method in their research on the CH_4–O_2 detonation with an elementary mechanism. Taylor *et al.*[36] also used this method in their simulation of H_2–O_2–Ar systems. Wang *et al.*[37] assessed the effects of spatially inhomogeneous mixtures on the local explosion and subsequent cellular detonation development. Xu *et al.*[38] studied the propagation and extinction of stoichiometric hydrogen/air detonations in fine water sprays.

In this paper, the effect of the mole weight ratio of the chemical reaction on the propagation of cellular detonation is investigated. A one-step reversible reaction is used to simulate the study object. For the chemical reaction of a gaseous mixture, the ratio of the mole weight of the reaction product to that of the reactant is a critical parameter for detonation initiation and propagation, but it has not been studied separately. For detailed reaction models, the mole weight is coupled with other parameters. For one-step and two-step models, the mole weight is set to be a fixed parameter, which is reflected in a fixed gas constant. For the chemical reaction of a gaseous mixture, the ratio of the mole weight of the reaction product to that of the reactant is a critical parameter for detonation initiation and propagation, but it has not been studied. In general, if the mole weight of a gaseous mixture decreases after a chemical reaction, the gaseous reactant has been dissociated to relatively smaller molecular products, as widely observed in the combustion of hydrocarbon fuel. On the contrary, if the mole weight of a gaseous mixture increases after a chemical reaction, then the gaseous reactant combines to form relatively larger molecular products, such as in hydrogen combustion. Here, we use a one-step reversible chemical reaction model for cellular detonation simulations with finite reaction rates. Given the average mole weight of the reactant W_A and the average mole weight of the product W_B, the ratio of the mole weight of the reaction W_B/W_A is introduced, and its effect on the propagation of cellular detonation is studied numerically.

II. PHYSICAL PROBLEM AND NUMERICAL METHOD

The geometry of the simulation domain is a two-dimensional channel of width 5 mm and length 125 mm. This is discretized on a 10 001 × 401 mesh. Initially, the high-temperature, high-pressure ignition region is located at the left side of the domain, and the remainder of the domain is full of a well-premixed combustible mixture. All boundaries are assigned inviscid slipping boundary conditions because viscosity is not very important for the directional initiation of high-energy detonation. The simulated physical model is shown in Fig. 1. After the detonation is initiated, the small disturbances behind the detonation front gradually increase and develop into transverse waves propagating perpendicular to the detonation front.

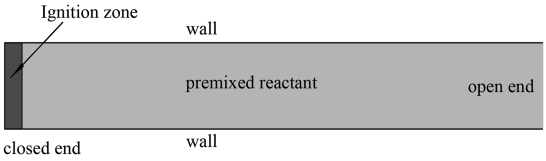

FIG. 1. Computational domain for detonation simulations.

Similar to previous studies,[39–42] the inviscid assumption is considered in the present study. The two-dimensional reactive Euler equations are solved numerically, and the one-step chemical reaction model is adopted. The Euler equations include the mass conservation equation, momentum equation, energy equation, and species equation. The one-step chemical reaction model uses a simplified hydrogen reaction model with three control parameters: chemical reaction heat Q, chemical reaction rate coefficient k_f, and chemical activation energy E_a. The control equations in the Cartesian coordinates are expressed as[43]

$$\frac{\partial \boldsymbol{U}}{\partial t} + \frac{\partial \boldsymbol{F}}{\partial x} + \frac{\partial \boldsymbol{G}}{\partial y} = \boldsymbol{S}, \tag{1}$$

$$\boldsymbol{U} = \begin{Bmatrix} \rho \\ \rho u \\ \rho v \\ \rho E \\ \rho \lambda \end{Bmatrix}, \ \boldsymbol{F} = \begin{Bmatrix} \rho u \\ \rho u^2 + p \\ \rho uv \\ u(\rho E + p) \\ \rho u \lambda \end{Bmatrix}, \ \boldsymbol{G} = \begin{Bmatrix} \rho v \\ \rho uv \\ \rho v^2 + p \\ v(\rho E + p) \\ \rho v \lambda \end{Bmatrix}, \ \boldsymbol{S} = \begin{Bmatrix} 0 \\ 0 \\ 0 \\ 0 \\ \rho \dot{\omega} \end{Bmatrix}, \tag{2}$$

where ρ, p, u, v, and E are the density, pressure, x and y components of velocity, and inner energy, respectively. λ represents the chemical reaction progress variable. $\dot{\omega}$ is the reaction source term of the reactive species. The inner energy E is formulated as

$$E = \frac{p}{\rho(\gamma - 1)} + \frac{1}{2}(u^2 + v^2) + (1 - \lambda)Q, \tag{3}$$

where γ is the constant specific heat ratio of the gas mixture. In this paper, the chemical reaction source term $\dot{\omega}$ of the one-step chemical reaction model is expressed as

$$\dot{\omega} = (1 - \lambda)k_f \exp\left(-\frac{E_a}{R_O T}\right) - \lambda k_b \exp\left(-\frac{E_a}{R_O T}\right), \tag{4}$$

where k_f and k_b represent the forward and reverse reaction rate coefficients, respectively. For a reversible chemical reaction, $k_b = k_f/\pi_e$,

where π_e is the equilibrium constant. E_a, R_O = 8.3143 (J/mol)/K, and T in the above-mentioned equation are the activation energy, general gas constant, and temperature, respectively. If $R_A = R_O/W_A$ and $R_B = R_O/W_B$ are given as the gas constants of the reactant and product, respectively, where W_A is the mole weight of the reactant and W_B is the mole weight of the product, then T is given by the following gas state equation:

$$p/\rho = [(1-\lambda)R_A + \lambda R_B]T. \tag{5}$$

The two-dimensional reactive Euler equations are numerically solved by the second-order nonoscillatory nonfree dissipative (NND) finite difference scheme.[44] The Steger–Warming flux vector splitting technology and minmod function are used to capture the shock discontinuity, which is effective in the numerical simulation of shock waves and detonation wave propagation. For the one-step chemical reaction model considered in this paper, the control parameters include k_f, π_e, E_a, Q, γ, W_A, and W_B, as well as the initial state parameters p_0, ρ_0, and T_0.

The parameters of the reactive gas ahead of the detonation are assigned as follows: initial pressure $p_0 = 1 \times 10^5$ Pa, initial temperature T_0 = 300 K, and gaseous specific heat ratio γ = 1.4, which are close to the properties of air under standard atmosphere conditions. The one-step chemical reaction model is parameterized as follows: reaction rate coefficient $k_f = 8.5 \times 10^8$, chemical equilibrium constant π_e = 0.05, activation energy $E_a = 2 \times 10^5$ J/mol, and chemical heat $Q = 1.58 \times 10^6$ kJ/kg. The dimensionless activation energy is approximately $\tilde{E}_a = E_a/R_O T_0 = 80.18$, and the dimensionless chemical heat is $\tilde{Q} = Q/R_A T_0 = 17.74$.

The mole weight of the reactant is selected as W_A = 0.028 kg/mol, and the mole weight of the product varies in the range W_B = 0.014–0.035 kg/mol, giving a mole weight ratio range of W_B/W_A = 0.57–1.25. The effect of the mole weight ratio of the chemical reaction on the propagation of cellular detonation is the focus of this paper. Artificial perturbations are not required because the numerical perturbations gradually grow and develop into strong perturbations if the computation domain is sufficiently long.

III. RESULTS AND DISCUSSION

A. Steady traveling wave solution for Zeldovich–von Neumann–Döring detonation

Before starting to investigate the two-dimensional numerical cases, the one-dimensional Zeldovich–von Neumann–Döring (ZND) detonation structure is first studied under different mole weight ratios W_B/W_A. As W_A is constant in this study, W_B/W_A is adjusted by changing W_B. The chosen chemical reaction model and parameters are almost consistent with the above-mentioned two-dimensional cases. However, the chemical reaction rate coefficient k_f is different, and it is adjusted such that the half-reaction zone has a unit length when W_B = 0.028 kg/mol. The chosen parameters are listed in Table I.

The ZND profiles for the pressure p, velocity u, reaction process λ, and heat release rate σ_R under different values of W_B are shown in Fig. 2. From Figs. 2(a) and 2(b), we find that the pressure and velocity of the Chapmen–Jouguet (CJ) state are the same for different values of W_B/W_A and their variation trends become gentler as W_B/W_A decreases. The chemical reaction process variable λ does not reach 1 because we consider a reversible reaction, as shown in Fig. 2(c). The reaction zone length is defined as the distance between the leading shock and the location of the 95% reaction process, marked in Fig. 2(c) by the colored dots. Obviously, the reaction zone length increases with increasing W_B/W_A. Figure 2(d) indicates that the rate of heat release is influenced by W_B/W_A and a decrease in W_B/W_A reduces the maximum of σ_R sharply. In addition, the distance between the location of maximal σ_R and the shock surface becomes longer. Therefore, the plots of the heat release rate tend to become flatter as W_B/W_A decreases. When the heat release rate is sufficiently small, the energy released per unit time is too small to support the self-sustaining propagation of the detonation wave. Thus, we have reason to speculate that the shock front will decouple from the chemical reaction and the detonation will be quenched when W_B/W_A reaches a certain threshold.

B. Categories of cellular detonation behaviors

As the average mole weight of product W_B varies from 0.016 to 0.035 kg/mol, i.e., the mole weight ratio of the chemical reaction W_B/W_A = 0.57–1.25, several typical and interesting cellular detonation behaviors can be observed in the numerical simulations. In the following numerical cases, the other control parameters of the chemical reaction, such as k_f, π_e, γ, E_a, and Q, are fixed, and only the effect of the mole weight ratio of the chemical reaction is considered. According to the cell patterns of stable detonation, the cellular detonation behaviors are divided into five categories according to the value of W_B: regular, relatively regular, irregular, half-cell propagating, and decoupled detonation, as shown in Table II. The behavior of each type of cellular detonation is now discussed.

1. Relatively regular propagating detonation

First, the case in which the mole weight is the same before and after the reaction is simulated, that is, the mole weight ratio W_B/W_A = 1.0. The cellular structures, instantaneous pressure, and density distributions are illustrated in Figs. 3(a)–3(c). After detonation initiation and a long period of detonation propagation, the small perturbations of the numerical simulation develop into strong transverse waves propagating along the detonation front. The cellular cells can be clearly identified by recording the local peak pressure history, which is created by the strong fluid shear interaction induced by the movements of triple points on the detonation front.

TABLE I. Summary of parameter settings.

R_O [(J/mol)/K]	T_0 (K)	W_A (kg/mol)	Ea^* (J/mol)	Ea	q^* (J/kg)	q	k_f
8.3143	300.0	0.028	2×10^5	80.2	1.58×10^6	17.75	156 773.4

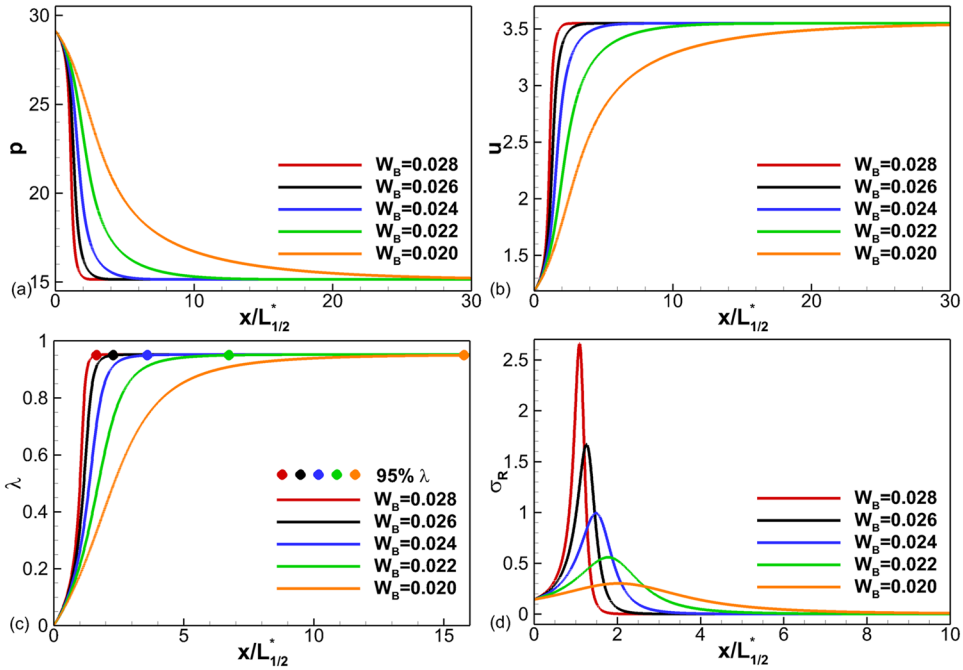

FIG. 2. ZND profiles of (a) pressure, (b) temperature, (c) reaction process, and (d) heat release rate.

The cellular structure is relatively regular over the whole flow field, although there exists local self-organized evolution of the detonation cell size due to the limit of the wall boundary conditions. The pressure distribution shown in Fig. 3(b) illustrates the strong transverse shock waves propagating along the detonation front. The density distribution shown in Fig. 3(c) illustrates the local complex wave structures near the triple points and the unreacted reactant behind the detonation wave.

Figure 4 presents the dimensionless peak pressure on the lower wall in the case of W_B/W_A = 1.0. During the initiation and evolution of numerical detonation, there are three distinct stages of evolution, that is, detonation ignition, unstable detonation, and stable detonation. In the detonation ignition stage, the perturbations in the flowfield are negligibly small. In the unstable detonation stage, the small numerical perturbations increase gradually, developing into strong disturbances in the flowfield and forming transverse waves on the detonation front. The fluctuations in peak pressure behind the detonation front are mainly caused by the strong interactions of transverse waves coupling with the collision of triple points on the detonation front. In the stable detonation stage, the fluctuations in peak pressure are rather periodic because of the relatively regular propagation of the leading detonation wave.

TABLE II. Categories of cellular structure under different values of W_B.

W_B	Cellular detonation
≥0.034	Regular
0.028–0.033	Relatively regular
0.019–0.027	Irregular
0.017–0.018	Half-cell propagating
≤0.016	Decoupled detonation

2. Regular propagating detonation

Next, we consider a numerical case with a high mole weight of the product W_B = 0.035 kg/mol, that is, the mole weight ratio of the product to the reactant is W_B/W_A = 1.25. The numerical simulations used the same control parameters of the chemical reaction and the same computational mesh. Figures 5(a)–5(c) show the numerical results in the current situation. From Fig. 5(a), we see that the fully developed detonation is quite regular but the cell size in this case is smaller than that for W_B/W_A = 1.0. After detonation ignition, the perturbations quickly develop into regularly propagating transverse waves. The regular detonation stage then maintains itself, and the cellular structures become quite uniform. From Figs. 5(b) and 5(c), it appears that the pressure and density are more uniform than those for W_B/W_A = 1.0 due to the smaller cell size.

Figure 6 shows the dimensionless peak pressure on the lower wall with W_B/W_A = 1.25. In the unstable detonation stage, the small numerical perturbations gradually increase and develop into strong disturbances, with transverse waves on the detonation front. The period of peak pressure fluctuations behind the detonation front is very short because of the small cell size of the detonation wave. Due to the limitations of the mesh resolution, the amplitude of the peak pressure fluctuations is smaller than that with lower mole weight ratios.

3. Irregular propagating detonation

Figure 7 shows the numerical detonation results for the case of W_B = 0.020 kg/mol, that is, the mole weight ratio W_B/W_A = 0.71.

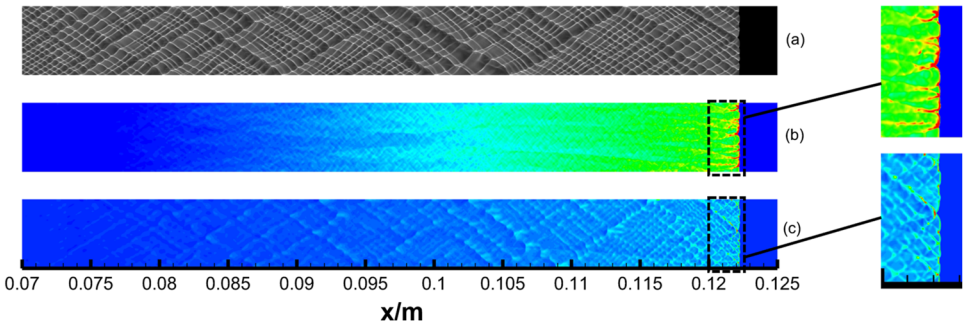

FIG. 3. Numerical detonation with the mole weight ratio W_B/W_A = 1.0. (a) Cellular structure; (b) pressure contours; (c) density contours.

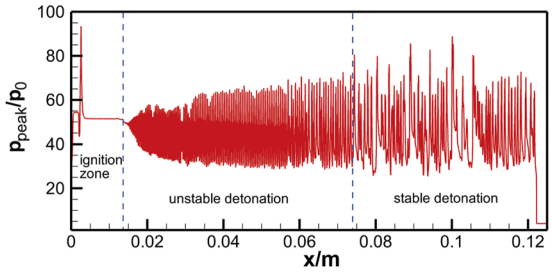

FIG. 4. Dimensionless peak pressure along the lower wall with W_B/W_A = 1.0.

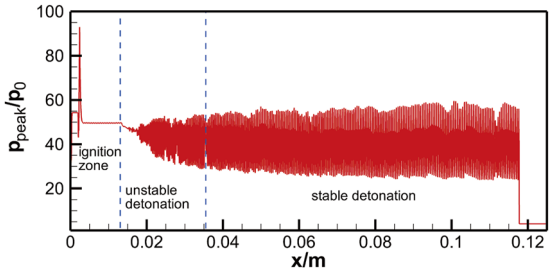

FIG. 6. Dimensionless peak pressure along the lower wall with W_B/W_A = 1.25.

In this situation, the mole weight of the product is lower than that of the reactant, representing the reactant being dissociated to relatively small molecules after the chemical reaction. According to the numerical results shown in Fig. 7(a), the cell size of stable detonation in this case is larger than that for W_B/W_A = 1.0. The conclusion is that the cells become larger as the mole weight of the chemical reaction product decreases. From the pressure and density distributions of the detonation flow field shown in Figs. 7(b) and 7(c), there are fewer transverse waves and triple points on the detonation front. The cellular structures recorded by the local pressure peak are not very regular, and there are several cellular modes, which correspond to cells of different sizes. With fewer triple points on the detonation front under the same channel width, the detonation front becomes more curved as the detonation cell size increases. In addition, the pressure and density are nonuniform behind the detonation front. Some eddies can even be observed in the downstream zone far from the wave front, as shown in Fig. 7(c).

Figure 8 shows the dimensionless peak pressure on the lower wall in the case of W_B/W_A = 0.71. The fluctuation period of fully developed detonation in this case is longer than that with a larger mole weight ratio. While the cell size of detonation increases, the fluctuation period increases with a lower mole weight ratio of the chemical reaction. During the initiation and evolution of numerical detonation, there are three distinct stages: detonation ignition, unstable detonation, and stable detonation. In the unstable detonation stage, the pressure fluctuations do not vary continuously. The nonlinear waves inducing the cellular detonation develop stage by stage, accompanied by the gradual recombination of cellular structures. The increase and development of the perturbation wave are rather nonlinear.

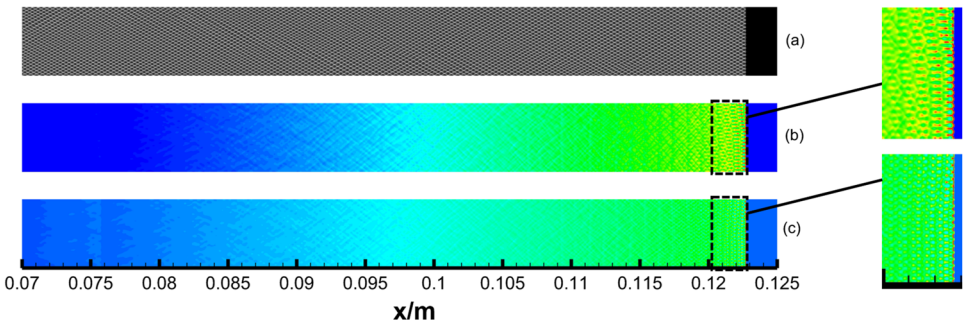

FIG. 5. Numerical detonation with the mole weight ratio W_B/W_A = 1.25. (a) Cellular structure; (b) pressure contours; (c) density contours.

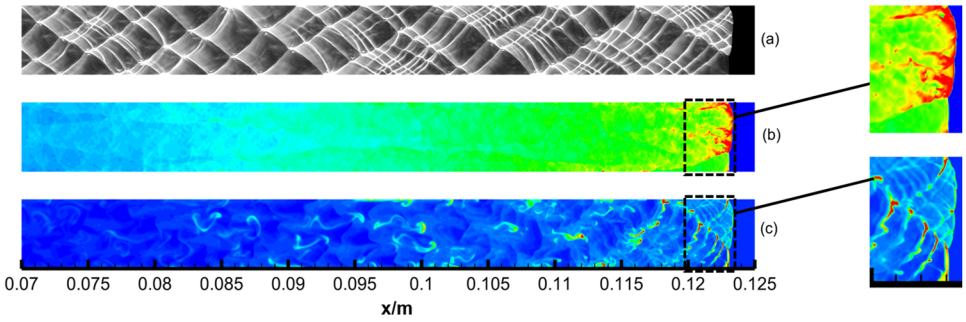

FIG. 7. Numerical detonation with the mole weight ratio W_B/W_A = 0.71. (a) Cellular structure; (b) pressure contours; (c) density contours.

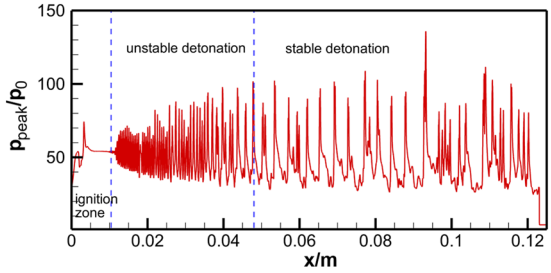

FIG. 8. Dimensionless peak pressure along the lower wall with W_B/W_A = 0.71.

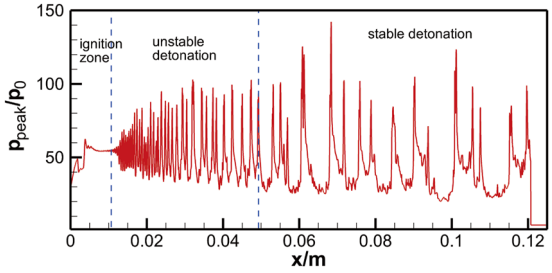

FIG. 10. Dimensionless peak pressure along the lower wall with W_B/W_A = 0.61.

4. Half-cell propagating detonation

Figure 9 shows the numerical results for the detonation wave in the case of W_B = 0.017 kg/mol, that is, the mole weight ratio W_B/W_A = 0.61. From Fig. 9(a), it can be seen that the detonation cells become rather irregular due to the limitations of the boundary of the duct. Only about half a cell can be observed at the exit of the duct, that is, the cell size of detonation at the exit is twice the duct width. This matches the "half-cell" law identified in Ref. 43. The evolution of the cellular structure is rather complex because nonlinear waves are generated in the flow field. As shown in Figs. 9(b) and 9(c), there is one dominant triple point on the detonation front moving between the boundary walls, which connects the incident shock to the Mach stem, transmitting shock, and shear layer. The propagation of detonation is mainly supported by the interaction of the shock wave, Mach stem, and chemical reaction wave. Behind the detonation front, there are many isolated reactant packets that have not reacted. The half-cell propagating detonation is a critical propagating state for cellular detonation. Any further increase in the cell size of detonation may cause the detonation to become decoupled to the point where it cannot sustain itself.

Figure 10 shows the dimensionless peak pressure on the lower wall in the case of half-cell propagating detonation. Large-amplitude pressure fluctuations can be observed, and the period of detonation oscillation increases significantly, which is very similar to the initiation and propagation of one-dimensional pulsating detonation waves.

5. Decoupled detonation limited by boundaries

When the mole weight ratio of the chemical reaction decreases further, the cell size of detonation for the given gaseous mixture will increase. Due to the limitations of the boundary walls of the

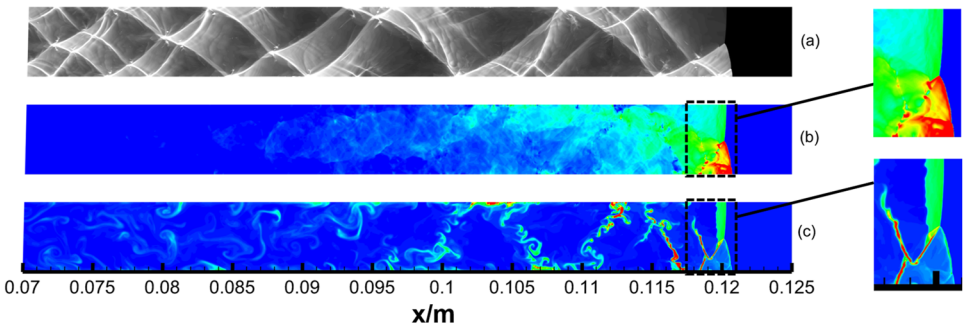

FIG. 9. Numerical detonation with the mole weight ratio M_B/M_A = 0.61. (a) Cellular structure; (b) pressure contours; (c) density contours.

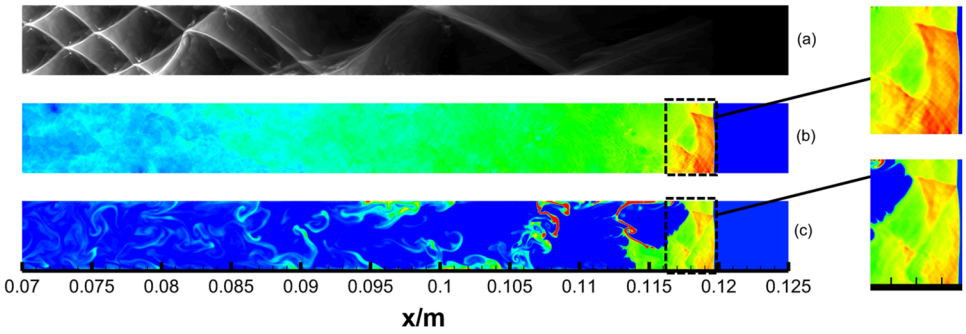

FIG. 11. Numerical detonation with the mole weight ratio W_B/W_A = 0.57. (a) Cellular structure; (b) pressure contours; (c) density contours.

duct, the detonation cannot be self-sustained. Figure 11 illustrates the detonation behavior in the case of W_B = 0.016 kg/mol, that is, the mole weight ratio W_B/W_A = 0.57. Initially, the detonation is directly ignited, and the chemical reaction is strongly coupled with the leading shock wave. The small perturbations of the numerical simulations then increase and develop into transverse waves propagating along the detonation front, whereupon the regular cellular detonation forms and adjusts itself to the proper cell size stage by stage. The collision of transverse waves with the wall boundary plays an important role in the splitting and recombination of the cellular structure. Finally, the cell size of detonation is too far beyond the width of the duct, and the collisions of transverse waves are suppressed. At this point, the chemical reaction is decoupled from the leading shock wave, and the detonation wave is gradually quenched. The numerical results show that the cellular detonation wave cannot sustain itself in when the width of the duct is less than half of the cell size of the detonation wave. Of course, this conclusion refers to the numerical conditions, and the energy loss by heat transfer on the wall is negligible.

Figure 12 shows the dimensionless peak pressure on the lower wall in the case of detonation decoupling. Periodic pressure fluctuations occur in the unstable detonation and regular detonation stages before the detonation reaches the position x = 0.08 m. After this point, the detonation begins to decouple, and the fluctuations in detonation pressure decay. Finally, the detonation pressure gradually weakens, indicating that the detonation is eventually quenched.

C. Correlation between one-dimensional ZND structure and two-dimensional cellular detonation

1. Effect of ZND parameters on cell size

According to the numerical investigation in Subsection III A, the cell size of detonation increases with the decreasing mole weight ratio of the chemical reaction over the range W_B/W_A = 0.57–1.25. The numerical simulation results can be correlated by showing the relationship between the cell size and mole weight ratio, as shown by the red line in Fig. 13. In addition, the reaction zone length and the maximum heat release rate σ_{Rmax} with respect to the mole weight ratio W_B/W_A are shown by the black and blue lines, respectively. The correlation covers the mole weight ratio range W_B/W_A = 0.57–1.0. The changes in the reaction zone length and cell size vs W_B/W_A exhibit good consistency. Larger values of W_B/W_A give a smaller reaction zone length, and the rate of decrease becomes smaller as W_B/W_A increases. However, the changes in the maximal heat release rate exhibit the opposite tendency. As W_B/W_A increases, the maximal heat release rate increases rapidly, which results in the closer coupling of the leading shock front and chemical reaction.

Numerical results for the temperature field with 95% λ contours (black solid lines) and the shock front (white solid lines) under different values of W_B are shown in Fig. 14. The reaction zone length is defined as the distance between the leading shock front and the

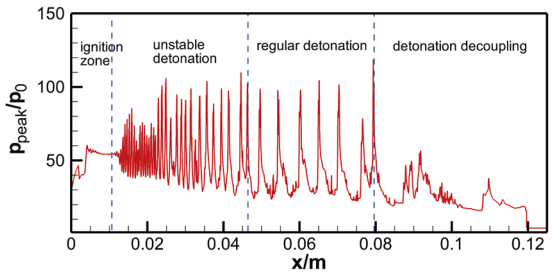

FIG. 12. Dimensionless peak pressure along the lower wall with W_B/W_A = 0.57.

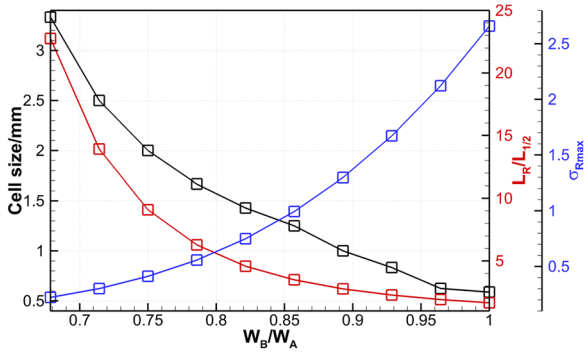

FIG. 13. Variation in cell size with respect to the mole weight ratio of the reaction.

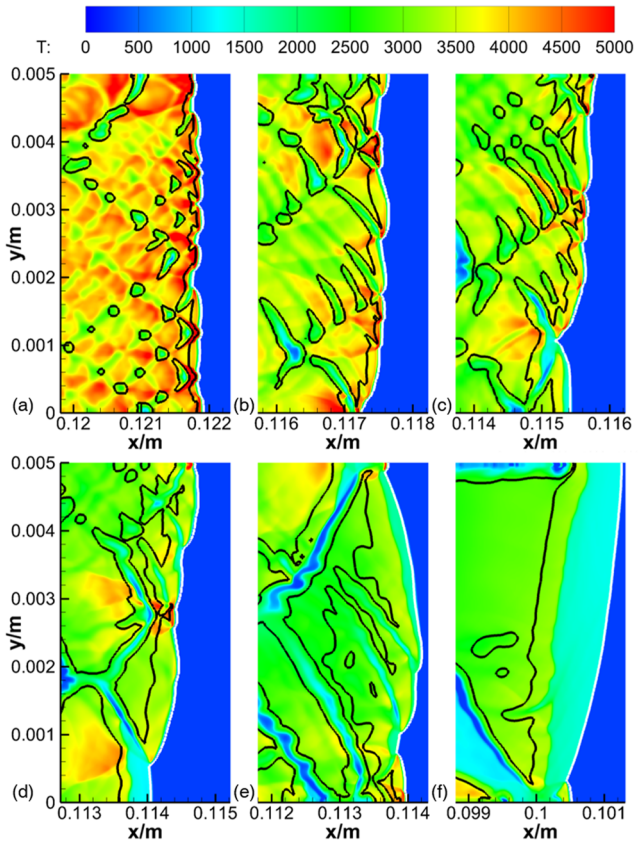

FIG. 14. Numerical results of pressure with 95% λ contours (black solid lines) and shock front (white solid lines) under different values of W_B/W_A: (a) 1.0, (b) 0.82, (c) 0.75, (d) 0.71, (e) 0.64, and (f) 0.57.

location of 95% λ, i.e., the distance between the black and white solid lines. Unlike the one-dimensional ZND structure, the reaction zone length is nonuniform along the direction of duct width because of the complex multi-wave structures on the detonation wave front. However, the macroscopic changes in the reaction zone length as W_B/W_A varies can be clearly observed. As W_B/W_A decreases, the reaction zone length increases, which is qualitatively consistent with the conclusion for the one-dimensional ZND structure. In addition, reducing W_B/W_A leads to a drop in temperature behind the leading shock wave. There are two main reasons for this. First, the temperature of the CJ state is significantly influenced by W_B/W_A. Second, the change in the heat release rate with W_B/W_A modifies the flow field temperature. Generally, a higher heat release rate will result in a higher temperature.

2. Thermoacoustic instability theory analysis of cell size

Thermoacoustic instability, also known as combustion instability,[45] is encountered in subsonic flow fields, such as in gas turbine boilers and aero engines. The theory is widely applied in the study of combustion instability phenomena in supersonic combustion ramjets (scramjets)[46–50] because various subsonic zones exist in scramjets, such as the boundary layer and recirculation zone. However, thermoacoustic instability theory has not been previously applied in the field of detonation.

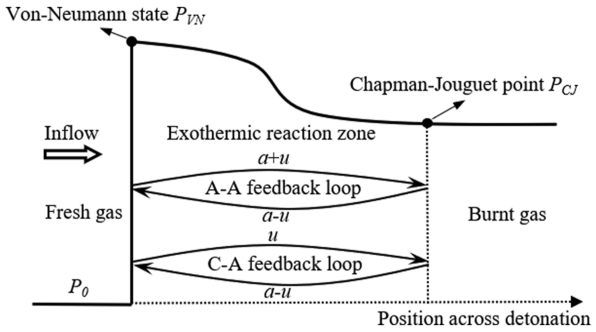

FIG. 15. Schematic representation of the pressure distribution across a CJ detonation with thermoacoustic instability modes.

The flow field in the reaction zone behind the leading shock is subsonic relative to the leading shock, which provides suitable conditions for applying thermoacoustic instability theory to detonation waves. As shown in Fig. 15, the instabilities are excited by the feedback loops between the leading shock and the end location of the exothermic reaction zone. There are two kinds of feedback loop in the reaction zone, i.e., the acoustic–acoustic (A–A) feedback loop and the convection–acoustic (C–A) feedback loop, as shown in Fig. 15. The former occurs because the small perturbance generated by unsteady heat release propagates to the shock front at sonic speed and interacts with the leading shock to create flow oscillations. These flow oscillations then propagate to the end location of heat release in the form of sound waves to enhance the unsteady heat release. In the propagation process of the small perturbations from the end location of heat release to the leading shock, the C–A feedback loop is the same as the A–A feedback loop. Differently, the flow oscillations propagate to the end location of heat release in the form of vortex waves and entropy waves, i.e., the propagation speed is only the flow field velocity u. Finally, the feedback forms a closed loop.

To investigate the characteristics of the two feedback loops quantitively and explore their relation with the cell size, the frequency of each kind of feedback loop is calculated as

$$f_{A--A} = \frac{1}{\int_{x_s}^{x_e} \frac{dx}{a+u} + \int_{x_s}^{x_e} \frac{dx}{a-u}}, \tag{6}$$

$$f_{C--A} = \frac{1}{\int_{x_s}^{x_e} \frac{dx}{u} + \int_{x_s}^{x_e} \frac{dx}{a-u}}, \tag{7}$$

where a, u, x_e, and x_s represent the sound velocity, flow field velocity, end location of the exothermic reaction zone, and location of the leading shock front, respectively. $f_{A\text{-}A}$ and $f_{C\text{-}A}$ are plotted with

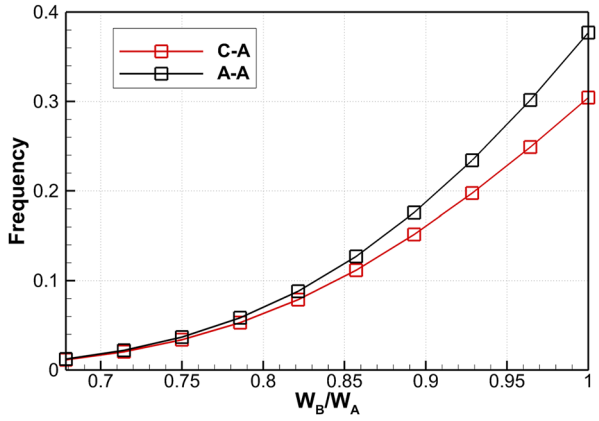

FIG. 16. Variation in feedback frequency with respect to the mole weight ratio of the reaction.

respect to the mole weight ratio W_B/W_A in Fig. 16. Both frequencies increase with increasing W_B/W_A. Higher frequencies enhance the perturbations and increase the maximal heat release rate, resulting in a reduction in cell size.

As a detonation propagates in a tube, its propagation behavior is strongly dependent on the boundary conditions. Therefore, we hope to find a parameter that includes the duct diameter D and cell size C_L. The ratio of D and C_L, that is, the cell number along the diameter of the tube, is considered as a parameter, and its correlation with the feedback frequencies is studied. A larger value of D/C_L produces a cellular detonation wave that is less affected by the duct wall. The relations between the cell number and feedback frequencies are shown in Fig. 17. Clearly, the cell number along the diameter of the duct increases with increasing frequency. The solid lines represent the linear fit of different frequencies and cell numbers. The linear fitting formula is $N_{cell} = af + b$, and the relevant parameters are listed in Table III.

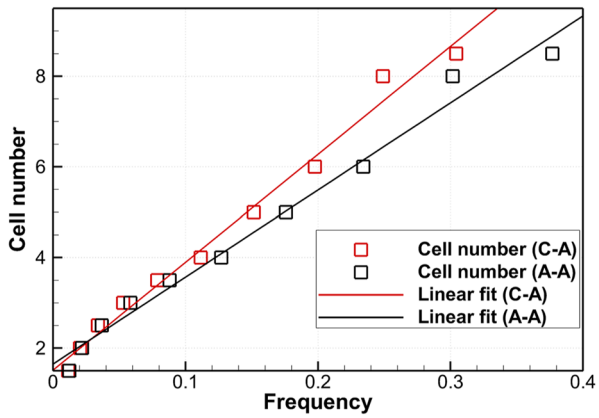

FIG. 17. Variation in feedback frequency with respect to the mole weight ratio of the reaction.

TABLE III. Relevant parameters of linear fitting formulas.

	a	b	SSE	R-square	RMSE
C-A	19.21	1.648	0.7439	0.9861	0.3049
A-A	23.81	1.515	0.6475	0.9879	0.2845

From Table III, it can be seen that the coefficients of determination (R-square) of the two kinds of frequencies are greater than 0.985, which indicates that the cell number has a strong linear dependence on the frequencies of the feedback loops. In addition, the root mean square error (RMSE) and the sum of the squared error (SSE) are both small, which demonstrates that the degree of dispersion between the cell number and linear fitting results is small. The R-square value for the A–A feedback loop is larger than that for the C–A feedback loop, and the SSE and RMSE of the A–A feedback loop are smaller than those of the C–A feedback loop. This shows that the A–A feedback loop has a greater influence on the cell number than the C–A feedback loop does.

3. Detonation speed defects under different mole weight ratios

Figure 18 shows the average speed of the detonation waves simulated in this paper. There are clearly detonation speed defects as the mole weight ratio of the chemical reaction decreases. These come from the increase in the cell size of the detonation waves and the increase in the number of unreacted mixture packets behind the detonation waves, as shown in Fig. 14. In the case of half-cell propagating detonation with large cell sizes, the detonation speed defects are much more serious and can reach about 10%. When the mole weight ratio decreases further, the shock wave front will decouple with the chemical reaction, and the detonation wave finally quenches because the detonation speed defects are too much. As the mole weight ratio increases, the cell size becomes smaller, and the cell shape becomes more uniform, as shown in Figs. 3 and 5. The

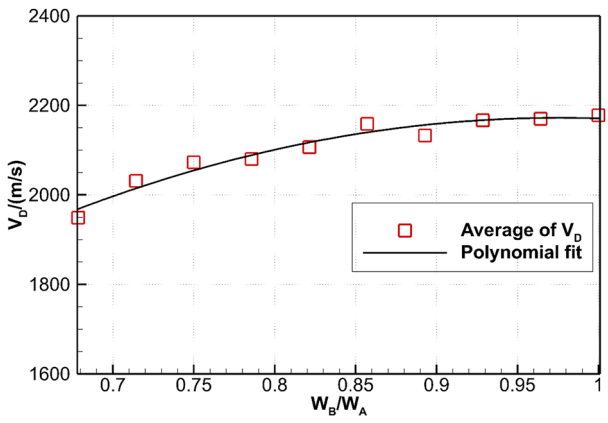

FIG. 18. Detonation speeds with respect to the mole weight ratio of the reaction.

increase rate of detonation speed with the mole weight ratio will become smaller. The detonation speed will tend to a fixed value in the end.

IV. CONCLUSIONS

The chemical reaction is vital in the initiation and propagation of cellular detonation. This paper has described a numerical investigation into the effect of the mole weight ratio of the product to the reactant on the behavior of cellular detonation. The parameter W_B/W_A was introduced to qualitatively study the ZND detonation structure and variations in the cell patterns of detonation waves in a duct of a certain width.

From the numerical results of cellular detonation propagation with different mole weight ratios, several detonation behaviors occur: regular, relatively regular, irregular, half-cell propagating, and decoupled detonation. The results also show that the detonation cell size depends on the mole weight ratio W_B/W_A of the chemical reaction, which can result in variations in cellular detonation behavior. To investigate the relationship between the cell size and W_B/W_A further, one-dimensional ZND detonation parameters were calculated, and two-dimensional numerical results were analyzed, showing that the mole weight ratio controls the cell size by influencing the reaction zone length. Larger values of W_B/W_A produce a smaller reaction region length and a smaller cell size. Thermoacoustic instability theory was introduced as a reasonable and innovative method for elucidating the effects of the reaction zone length on the cell size. The results show that acoustic perturbations play an important role in the instability of the cellular detonation front. The correlation between the propagation frequencies of the perturbations and the cell number along the width of the duct was then derived. Correlation analysis indicates that the cell number has a strong linear dependence on the frequencies of these perturbations.

Based on the above-mentioned analysis, the effect of the mole weight ratio should be considered in simulations of detonation waves with simplified chemical reaction models to ensure appropriate behavior of gaseous detonation waves. As the detonation cell size increases, obvious detonation speed defects are produced by the increase in the number of unreacted mixture packets behind the detonation waves.

ACKNOWLEDGMENTS

This work has been supported by the National Natural Science Foundation of China (Grant Nos. 12072353 and 12132017).

AUTHOR DECLARATIONS

Conflict of Interest

The authors have no conflicts to disclose.

Author Contributions

Haoyang Li: Software (lead); Validation (lead); Visualization (equal); Writing – original draft (lead); Writing – review & editing (lead). **Kepeng Yao**: Software (supporting); Validation (equal). **Ruixin Yang**: Investigation (equal); Software (equal). **Chun Wang**: Resources (lead); Software (lead); Supervision (lead); Writing – review & editing (supporting).

DATA AVAILABILITY

The data that support the findings of this study are available from the corresponding author upon reasonable request.

APPENDIX: GRID RESOLUTION TEST

In the paper, we choose $W_B/W_A = 1.0$ as a benchmark case to carry out grid resolution test. As shown in Fig. 19, the grid sizes $\Delta x = L_{1/2}/7.5$, $\Delta x = L_{1/2}/15$, and $\Delta x = L_{1/2}/30$ are performed and discussed; here, $L_{1/2}$ represents the half-reaction zone length. As in the study by Lu *et al.*,[51] the release heat zone length $L_{hr} = 0.4\ L_{1/2}$ in this case, that is, the grid sizes $\Delta x = L_{hr}/3$, $\Delta x = L_{hr}/6$, and $\Delta x = L_{hr}/12$ are shown in Fig. 19. According to previous work by Choi *et al.*,[52] a minimum of five grid points should be included in the heat-release zone in order to achieve an accurate simulation of detonation cell structures. From Fig. 19(a), it can be seen that for the lowest resolution, the cells are nearly uniform and unclear. Further refinement shows that secondary shocks start to appear, which increases the irregularity of the cellular structure. Nonetheless, cell widths of primary cells with clearer boundaries are close, as shown in Figs. 19(b) and 19(c), when the grid spacing is halved. With increasing resolution, the numerical simulation may reveal a secondary cellular structure within the primary detonation cells. However, the multilevel cell structure is beyond the scope of this work.

Figure 20 shows the cell size distributions under different grid sizes in the domain shown in Fig. 19. These were obtained by manually measuring all the cell sizes (50 samples per case) and subsequently sorting the data by the number of occurrences of a given scale, i.e., frequency (#). From Fig. 20, it can be seen that the cell size distributions of $\Delta x = L_{1/2}/7.5$ and $\Delta x = L_{1/2}/15$ are very different while the cell size distributions of $\Delta x = L_{1/2}/15$ and $\Delta x = L_{1/2}/30$ are similar. Besides, the difference in the average cell size of $\Delta x = L_{1/2}/15$ and $\Delta x = L_{1/2}/30$ is smaller than $\Delta x = L_{1/2}/7.5$ and $\Delta x = L_{1/2}/15$. Therefore, the grid size $\Delta x = L_{1/2}/15$ is adopted in our study. This shows an influence of grid resolution similar to that reported in Ref. 52. Therefore, the resolution requirement proposed by Ref. 52 indeed holds true and is used throughout this work.

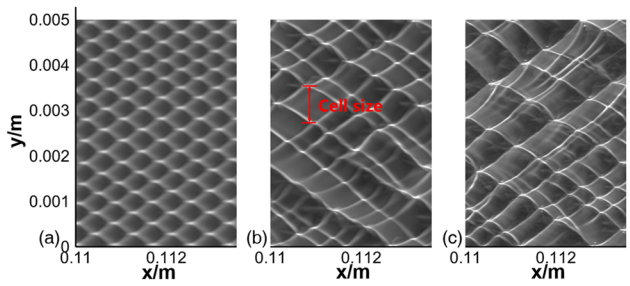

FIG. 19. Numerical smoke foils under different grid sizes: (a) $\Delta x = L_{1/2}/7.5 = L_{hr}/3$; (b) $\Delta x = L_{1/2}/15 = L_{hr}/6$; (c) $\Delta x = L_{1/2}/30 = L_{hr}/12$.

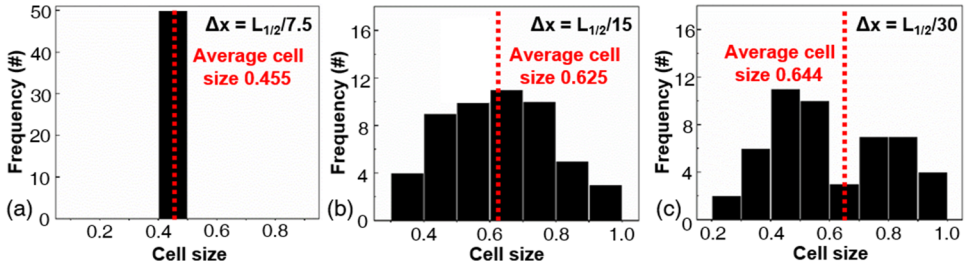

FIG. 20. Cell size distributions under different grid sizes: (a) $\Delta x = L_{1/2}/7.5 = L_{hr}/3$; (b) $\Delta x = L_{1/2}/15 = L_{hr}/6$; (c) $\Delta x = L_{1/2}/30 = L_{hr}/12$.

REFERENCES

[1] J. H. S. Lee, *The Detonation Phenomenon* (Cambridge University Press, Cambridge, 2008).

[2] G. D. Roy, S. M. Frolov, A. A. Borisov, and D. W. Netzer, "Pulse detonation propulsion: Challenges, current status, and future perspective," Prog. Energy Combust. Sci. **30**, 545–672 (2004).

[3] F. Zhang, *Shock Wave Science and Technology Reference Library* (Springer, Berlin, 2009).

[4] W. Fickett and W. C. Davis, *Detonation: Theory and Experiment* (Courier Corporation, 2000).

[5] G. J. Sharpe, "Transverse waves in numerical simulations of cellular detonations," J. Fluid Mech. **447**, 31–51 (2001).

[6] R. A. Strehlow and F. D. Fernandes, "Transverse waves in detonations," Combust. Flame **9**, 109–119 (1965).

[7] Q. Xiao and C. Weng, "Effect of losses on hydrogen–oxygen–argon detonation cell sizes," Phys. Fluids **33**, 116103 (2021).

[8] B. Zhang, H. Liu, B. Yan, and H. D. Ng, "Experimental study of detonation limits in methane-oxygen mixtures: Determining tube scale and initial pressure effects," Fuel **259**, 116220 (2020).

[9] Y. N. Denisov, "Pulsating and spinning detonation of gaseousmixtures in tubes," Dokl. Akad. Nauk SSSR **125**, 110–113 (1959).

[10] M. I. Radulescu, G. J. Sharpe, C. K. Law, and J. H. S. Lee, "The hydrodynamic structure of unstable cellular detonations," J. Fluid Mech. **580**, 31–81 (2007).

[11] W. H. Han, J. Huang, N. Du, Z. G. Liu, W. J. Kong, and C. Wang, "Effect of cellular instability on the initiation of cylindrical detonations," Chin. Phys. Lett. **34**, 054701 (2017).

[12] J. H. S. Lee, "Dynamic parameters of gaseous detonations," Annu. Rev. Fluid Mech. **16**, 311–336 (1984).

[13] R. Knystautas, J. H. Lee, and C. M. Guirao, "The critical tube diameter for detonation failure in hydrocarbon-air mixtures," Combust. Flame **48**, 63–83 (1982).

[14] S. M. Frolov and B. E. Gel'fand, "Limit diameter of gas detonation propagation in tubes," Combust., Explos. Shock Waves **27**, 113–117 (1991).

[15] G. Dong, B. C. Fan, and Y. L. Chen, "Acceleration of chemistry computations in two-dimensional detonation induced by shock focusing using reduced ISAT," Combust. Theory Modell. **11**, 823–837 (2007).

[16] X. Xi, H. Teng, Z. Chen, and P. Yang, "Effects of longitudinal disturbances on two-dimensional detonation waves," Phys. Rev. Fluids **7**, 043201 (2022).

[17] X. Q. Yuan, C. Yan, J. Zhou, and H. D. Ng, "Computational study of gaseous cellular detonation diffraction and re-initiation by small obstacle induced perturbations," Phys. Fluids **33**, 047115 (2021).

[18] P. Yang, H. Teng, H. D. Ng, and Z. Jiang, "A numerical study on the instability of oblique detonation waves with a two-step induction–reaction kinetic model," Proc. Combust. Inst. **37**, 3537–3544 (2019).

[19] G. X. Xiang, X. Gao, W. J. Tang, X. Z. Jie, and X. Huang, "Numerical study on transition structures of oblique detonations with expansion wave from finite-length cowl," Phys. Fluids **32**, 056108 (2020).

[20] P. Yang, H. D. Ng, and H. Teng, "Numerical study of wedge-induced oblique detonations in unsteady flow," J. Fluid Mech. **876**, 264–287 (2019).

[21] P. Yang, H. Teng, Z. Jiang, and H. D. Ng, "Effects of inflow Mach number on oblique detonation initiation with a two-step induction-reaction kinetic model," Combust. Flame **193**, 246–256 (2018).

[22] V. N. Gamezo, D. Desbordes, and E. S. Oran, "Formation and evolution of two-dimensional cellular detonations," Combust. Flame **116**, 154–165 (1999).

[23] V. N. Gamezo, D. Desbordes, and E. S. Oran, "Two-dimensional reactive flow dynamics in cellular detonation waves," Shock Waves **9**, 11–17 (1999).

[24] A. V. Trotsyuk, "Numerical simulation of the structure of two-dimensional gaseous detonation of an H_2-O_2-Ar mixture," Combust., Explos. Shock Waves **35**, 549–558 (1999).

[25] G. J. Sharpe and J. J. Quirk, "Nonlinear cellular dynamics of the idealized detonation model: Regular cells," Combust. Theory Modell. **12**, 1–21 (2008).

[26] Y.-T. Shao, M. Liu, and J.-P. Wang, "Numerical investigation of rotating detonation engine propulsive performance," Combust. Sci. Technol. **182**, 1586–1597 (2010).

[27] E. S. Oran, J. P. Boris, T. Young, M. Flanigan, T. Burks, and M. Picone, "Numerical simulations of detonations in hydrogen-air and methane-air mixtures," Symp. (Int.) Combust. **18**, 1641–1649 (1981).

[28] C. K. Westbrook and P. A. Urtiew, "Chemical kinetic prediction of critical parameters in gaseous detonations," Symp. (Int.) Combust. **19**, 615–623 (1982).

[29] J. E. Shepherd, "Chemical kinetics of hydrogen-air-diluent detonations. [Kinetic models to predict detonation cell size]," Technical Report No. SAND-85-0547C, Sandia National Laboratories, Albuquerque, NM, 1985.

[30] R. K. Kumar, "Detonation cell widths in hydrogen oxygen diluent mixtures," Combust. Flame **80**, 157–169 (1990).

[31] S. Taileb, J. Melguizo-Gavilanes, and A. Chinnayya, "The influence of the equation of state on the cellular structure of gaseous detonations," Phys. Fluids **33**, 036105 (2021).

[32] E. S. Oran, J. W. Weber, Jr., E. I. Stefaniw, M. H. Lefebvre, and J. D. Anderson, Jr., "A numerical study of a two-dimensional H_2-O_2-Ar detonation using a detailed chemical reaction model," Combust. Flame **113**, 147–163 (1998).

[33] K. Shchelkin and Y. K. Troshin, *Gas Dynamics of Combustion* (Mono Book Corp, Baltimore, 1965).

[34] A. I. Gavrikov, A. A. Efimenko, and S. B. Dorofeev, "A model for detonation cell size prediction from chemical kinetics," Combust. Flame **120**, 19–33 (2000).

[35] R. Eaton, B. Zhang, J. M. Bergthorson, and H. D. Ng, "Measurement and chemical kinetic model predictions of detonation cell size in methanol-oxygen mixtures," Shock Waves **22**, 173–178 (2012).

[36] B. D. Taylor, D. A. Kessler, V. N. Gamezo, and E. S. Oran, "Numerical simulations of hydrogen detonations with detailed chemical kinetics," Proc. Combust. Inst. **34**, 2009–2016 (2013).

[37] Y. Wang, Z. Chen, and H. Chen, "Propagation of gaseous detonation in spatially inhomogeneous mixtures," Phys. Fluids **33**, 116105 (2021).

[38] Y. Xu, M. Zhao, and H. Zhang, "Extinction of incident hydrogen/air detonation in fine water sprays," Phys. Fluids **33**, 116109 (2021).

[39] Y. Zhang, L. Zhou, J. Gong, H. D. Ng, and H. Teng, "Effects of activation energy on the instability of oblique detonation surfaces with a one-step chemistry model," Phys. Fluids **30**, 106110 (2018).

[40] P. Yang, H. D. Ng, H. Teng, and Z. Jiang, "Initiation structure of oblique detonation waves behind conical shocks," Phys. Fluids **29**, 086104 (2017).

[41] H. Li, W. Han, J. Li, and W. Fan, "Influences of incoming flow on re-initiation of cellular detonations," Combust. Flame **229**, 111376 (2021).

[42]G. Q. Zhang, S. F. Gao, and G. X. Xiang, "Study on initiation mode of oblique detonation induced by a finite wedge," Phys. Fluids **33**, 016102 (2021).
[43]C. Wang, Z. L. Jiang, and Y. L. Gao, "Half-cell law of regular cellular detonations," Chin. Phys. Lett. **25**, 3704–3707 (2008).
[44]H. Zhang and F. Zhuang, "NND schemes and their applications to numerical simulation of two- and three-dimensional flows," Adv. Appl. Mech. **29**, 193–256 (1991).
[45]X. Sun and X. Wang, *Fundamentals of Aeroacoustics with Applications to Aeropropulsion Systems*, Elsevier and Shanghai Jiao Tong University Press Aerospace Series (Elsevier, 2020).
[46]F. Ma, J. Li, V. Yang, K. C. Lin, and T. Jackson, "Thermoacoustic flow instability in a scramjet combustor," in 41st AIAA/ASME/SAE/ASEE Joint Propulsion Conference and Exhibit, Tucson, AZ, 10–13 July 2005.
[47]J. Li, F. Ma, V. Yang, K. C. Lin, and T. Jackson, "A comprehensive study of combustion oscillations in a hydrocarbon-fueled scramjet engine," in 45th AIAA Aerospace Sciences Meeting and Exhibit, Reno, NV, 8–11 January 2007.
[48]K. C. Lin, K. Jackson, R. Behdadnia, T. A. Jackson, F. Ma, J. Li, and V. Yang, "Acoustic characterization of an ethylene-fueled scramjet combustor with a rectangular cavity flameholder," in 43rd AIAA/ASME/SAE/ASEE Joint Propulsion Conference and Exhibit, Cincinnati, OH, 8–11 July 2007.
[49]K.-C. Lin, K. Jackson, R. Behdadnia, T. A. Jackson, F. Ma, and V. Yang, "Acoustic characterization of an ethylene-fueled scramjet combustor with a cavity flameholder," J. Propuls. Power **26**, 1161–1170 (2010).
[50]Z.-g. Wang, M.-b. Sun, H.-b. Wang, J.-f. Yu, J.-h. Liang, and F.-c. Zhuang, "Mixing-related low frequency oscillation of combustion in an ethylene-fueled supersonic combustor," Proc. Combust. Inst. **35**, 2137–2144 (2015).
[51]X. Lu, C. R. Kaplan, and E. S. Oran, "A chemical-diffusive model for simulating detonative combustion with constrained detonation cell sizes," Combust. Flame **230**, 111417 (2021).
[52]J. Y. Choi, F. H. Ma, and V. Yang, "Some numerical issues on simulation of detonation cell structures," Combust., Explos. Shock Waves **44**, 560–578 (2008).